Autonomous robotic system for breast biopsy with deformation compensation

Sandro Ferrari, Eleonora Tagliabue, Bogdan Mihai Maris, Paolo Fiorini

Abstract— **Image-guided biopsy is the most common technique for breast cancer diagnosis. Although magnetic resonance imaging (MRI) has the highest sensitivity in breast lesion detection, ultrasound (US) biopsy guidance is generally preferred due to its non-invasiveness and real-time image feedback during the insertion. In this work, we propose an autonomous robotic system for US-guided biopsy of breast lesions identified on pre-operative MRI. After initial MRI to breast registration, the US probe attached to the robotic manipulator compresses the breast tissues until a pre-determined force level is reached. This technique, known as preloading, will allow to minimize lesion displacement during the needle insertion. Our workflow integrates a deformation compensation strategy based on patient-specific biomechanical model to update the US probe orientation keeping the target lesion on the US image plane during compression. By relying on a deformation model, the proposed system does not require lesion visibility on US. Experimental evaluation is performed to assess the performance of the system on a realistic breast phantom with 15 internal lesions, considering different preloading forces. The deformation compensation strategy allows to improve localization accuracy, and as a consequence final probe positioning, for all considered lesions. Median lesion localization error is 3.3 mm, which is lower than the median lesion radius, when applying a preloading of 2 N, which guarantees both minimal needle insertion error and tissue stress.**

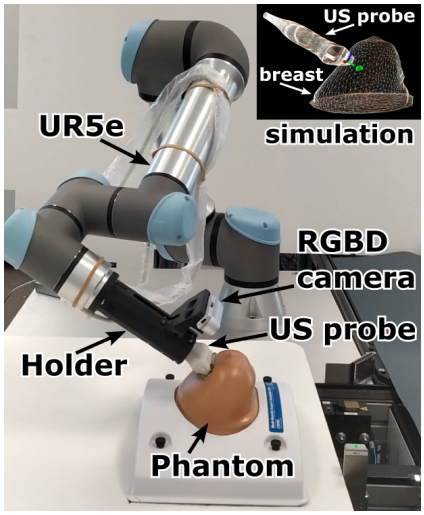

Fig. 1: The experimental setup. It includes a 6-DOFs robot holding the US probe and RGB-D camera, and a realistic breast phantom. Lesion displacement due to US probe compression is estimated with a patient-specific biomechanical model, shown in the upper right corner.

I. Introduction

Breast cancer is the most common cancer among women [1]. Timely identification and analysis of suspicious breast lesions is critical to reduce the impact of the disease. Although several imaging techniques are available to detect suspicious lesions, such as mammography, MRI and US, the only way to confirm the nature of the lesion is tissue biopsy. The biopsy procedure consists in the collection and analysis of a sample of cells from the suspicious lesion obtained with a needle. Proper needle steering towards the target is achieved by performing the procedure under image guidance (MRI, X-rays or US). Although MRI has the highest sensitivity for breast lesion detection, it does not provide real-time image feedback. Moreover, MRI-guided biopsy is limited by the cost, the long procedure time, the need for experienced staff and specific equipment, the use of intravenous contrast medium and the limited accessibility to the target lesion [2]. Stereotactic biopsy (i.e., X-rays based) is also challenging, painful due to the necessary compression, and invasive for the patient due to the resulting radiation burden. US-guided biopsy is the preferred method as it allows real-time visualization of the needle without using ionizing radiations, paddle compression or contrast injection [3]. However, the low US image quality often hinders the detection of small lesions, which might be not visible in US [4]. In these cases, the manual biopsy, under US guidance, is based on the fusion made by an experienced physician through the cognitive mapping of pre-operatively identified target in MRI or mammography to the real-time US image seen on the monitor. In the field of breast MRI automatic registration, an important result was published in [5]. Here, the authors used free form deformations based on B-splines to register the MRI images acquired from the same patient in two different moments in time. The deformation was caused by patient movement. Prone to supine registration of MRI and Computer Tomography was presented in [6]. However, the multimodal registration of US images acquired under the pressure of the probe and MRI images for a breast biopsy procedure is still a research subject.

Instead of directly registering the images, our idea is to use a biomechanical model of the breast and a deformation compensation algorithm to accurately predict the displacements of the tumors beforehand. In this context, the use of the robot is of paramount importance since it can reach a predefined

Authors are with the Department of Computer Science, University of Verona, 37134 Verona, Italy. Corresponding author: bogdan.maris@univr.it

The present contribution is supported by the European Research Council (ERC) under the European Union's Horizon 2020 research and innovation programme under grant agreement No. 742671 (ARS).

level of compression force through constant and controlled increments. The ultimate challenge that our system can solve is targeting small lesions while following their movement during the interaction with the US probe. Moreover, with this system we want to reach and control a constant force that allows the optimal insertion of the biopsy needle without further deformation of the tissue.

The implementation of this innovative approach required the realization of a complete robotic system (Fig. 1) and a workflow that we describe below.

In the proposed method, suspicious lesions are identified on a pre-operative MRI and their positions are then mapped to the reference system of the robot already calibrated with the US image. Reliance on MRI allows to improve the sensitivity of the setup, detecting also those lesions which are not visible on US. The presence of a robotic manipulator allows to increase not only the precision but also the repeatability of the procedure [7].

The specific contributions of this paper are:

1) an autonomous robot-assisted US-guided breast biopsy system that performs the procedure from initial image registration to the final positioning of the US probe, just before needle insertion;
2) a parallel force-position control used to apply a compression that minimizes lesion displacement at needle insertion time, while continuously keeping the lesion on the image plane.
3) A dedicated software to implement a deformation compensation scheme for the tracking of lesion displacement due to the probe compression; the software is publicly available at https://gitlab.com/altairLab/robotic_breast_deformation_compensation

The following sections begin with the review of related works for robot-assisted US-guided biopsy (Section II). We present our setup and our pipeline in Section III. Section IV describes the experimental evaluation and the results we obtained. Discussion is reported in Section V, while conclusions and future works are summarized in Section VI.

II. Background

The use of a robotic manipulator to automate US scanning has been proposed to improve image acquisition, to facilitate volumetric reconstruction or to achieve optimal probe positioning, in different medical applications [8], [9]. Robot-assisted systems for US-guided biopsy have been recently surveyed in [7]. In the context of the breast, most of the existing systems employ the robotic manipulator to stabilize needle holding during the insertion phase [10]. A recent overview of image-guided interventional robotics with references to US guided robots was published in [11]. Welleweerd et al. proposed to autonomously acquire a set of 2D US images with a 6-DOF robot for 3D US volume reconstruction, following a trajectory that is adapted to each patient [12]. This approach focuses on the optimization of acoustic coupling which minimizes breast deformation during image acquisition, but does not address the needle insertion phase. Other systems, such as [13] and [14], have been developed for autonomous acquisition and reconstruction of a 3D breast ultrasound volume. However, these approaches rely on specific hardware that cannot be easily integrated with a robotic biopsy setup, thus making these systems usable for lesion detection only. Moreover, such systems deform the anatomy during acquisition, making the registration with pre-operative MRI cumbersome. An area of application where the integration of 3D US imaging and robotic guidance may lead to autonomous systems is the robotic prostate biopsy [15]. A complete review of the existing autonomous capabilities of surgical robots with the introduction of a practical scale to assess the level of autonomy of current and future surgical robots may be found in [16], [17].

Some strategies to compensate for tissues deformation due to US probe compression based on optical flow or confidence maps have been proposed in the context of blood vessel scanning [8], [18], [19]. Only few works have integrated methods to compensate for probe-induced deformations during robotic breast US scanning. In [20], the authors introduce a complete robotic setup for US-guided biopsy of lesions detected on a pre-operative MRI, and probe-induced lesion displacement is estimated using optical flow. This approach does not allow to track out-of-plane lesion movements, and it has been tested on a simplistic phantom which only allows very small deformation. Some works have proposed to track the displacement of internal breast targets due to US probe compression during freehand US using patient-specific deformation models [21], [22]. Groenhuis et al. have incorporated a biomechanical model within a robotic setup for breast biopsy to compensate for probe-induced deformations [23]. A robotic setup and software architecture to assist the radiologist in targeting suspicious tumours under MRI guidance was published in [24].

There is no strategy to minimize the needle positioning error in this work, therefore the results were not clinically satisfactory in all the tested conditions. In fact, some research works have demonstrated that needle insertion accuracy can be significantly improved if an additional compression is applied to the breast tissue with the US probe [25], [26]. In particular, such error decreases with increasing tissue compression up to a threshold identified in [26] as 2N. This compression is called *preloading*. Other frameworks that implement a variety of needle insertion techniques and configurations were published in [27].

III. Method

One of the assumptions in the proposed workflow is that the patient lies in the same position during the robotic procedure as it was in the pre-operative MRI scanning, similarly to [12], [20]. This will reduce the errors due to patient repositioning. In MRI acquisition, the patient lies on the bed in prone position with bare breasts in a dedicated compartment. The robotic manipulator is positioned at the side of the patient's bed, and a US probe and a depth camera are attached to its end-effector. The workflow begins with the segmentation of the breast surface and of the suspicious

lesions on the pre-operative MRI image through a semi-automatic method [28]. Just before the biopsy procedure, initial registration is performed to map information from MRI to the current patient position. Afterwards, the robot moves to the optimal location on the breast surface to reach the lesion with the biopsy needle. The robot then starts to compress the breast with the US probe until the applied pressure reaches the desired level of preloading. The probe will deform the tissue during compression. Therefore, we integrate a deformation compensation scheme that relies on a patient-specific biomechanical model and allows to continuously track lesions movement and adjust the US probe orientation during preloading. In this way, when the target preloading force is applied, the probe is positioned such that the lesion lies on the US image plane. This allows to observe the needle in real time on the US image during the biopsy needle insertion. Pipeline details are presented in the following subsections.

A. Initial registration

A registration phase is needed to map the information extracted from the pre-operative MRI images to the current breast position. The registration pipeline is markerless and fully automatic, thus simplifying the operator's workflow. Just before the biopsy, the breast anatomy is localized in the robot reference frame using the camera mounted on the robot end-effector. As a first step, the robot is placed below the breast anatomy to acquire a point cloud that includes the lowest breast points, i.e., around the nipple. The centroid of this point cloud represents the center of a circular trajectory that the robot will follow, and corresponds to the point that the camera will always look at. Current breast shape is reconstructed by composing multiple point clouds acquired from different viewpoints while the robot moves on this trajectory. The segmentation of the acquired point clouds is based on color selection, in order to keep points belonging to the breast skin surface only, following the approach described in [29]. A masking based on the breast bounding box is then applied to remove possible outlier points. The bounding box is a cube centered in the estimated centroid of the breast and with sides twice as long as the maximum size of the breast model extracted from the MRI. The composition of the different point clouds is immediate since they lie in the robot coordinate system.

Before estimating the registration transformation, the breast surface reconstructed from the point cloud and the breast surface from segmentation of the pre-operative 3D model are voxelized relying on the same parameters, in order to obtain uniform spatial distribution and discretization of points in the two conditions. Iterative Closest Point (ICP) algorithm [30] is then used to find the rigid transformation that aligns the pre-operative and intra-operative breast shape given as point clouds.

To increase the success of ICP by avoiding local minima due to large rotations and symmetry of the shape, after the initial alignment based on centroids, the point cloud is rotated for 360 degrees around the vertical axis. We assume that the vertical axis of the two points clouds is similar, since the breast base is upward and it is falling downward in both instances (pre- and intra-operative). The rotation is performed every 10 degrees and ICP is launched after each rotation.

After a complete set of rotations, the pose where the algorithm reached the minimum error will be chosen as the initial transformation. This transformation allows to map the positions of lesions detected in MRI to the robot reference system, before any physical interaction takes place.

B. Breast approach

Once registration is complete, the robot moves to the desired contact point $\mathbf{P}$ on the breast surface, as shown in Fig. 2. $\mathbf{P}$ is defined as the closest point on the breast surface to the centroid $\mathbf{X}$ of the suspicious lesion. The US probe is oriented along a direction $\mathbf{d}$ such that the center of the US image plane (i.e., the US probe y-axis in Fig. 2) intersects with $\mathbf{X}$, thus maximizing the probability to include the lesion in the US image plane. As additional constraints, the orientation of the end-effector is defined such that the probe x-axis is parallel to the patient's bed, and the camera lies farther away from the stretcher with respect to the probe (see Fig. 1). This constrain allows to maximize the adherence between the US sensor and the patient's skin leading to improved image quality and uniform pressure distribution at the contact interface, as shown in [20]. Furthermore, the robot trajectory to reach $\mathbf{P}$ is generated to avoid unwanted collisions with the anatomy. To ensure this, robot motion is constrained to pass through an intermediate pose before reaching $\mathbf{P}$. Such pose is defined along the direction going from the inner lesion to $\mathbf{P}$, and outside of the breast surface.

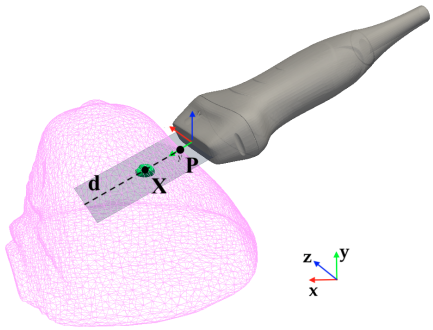

Fig. 2: US probe positioning during breast approach. The US image plane is shown in gray, while the target lesion is green. $\mathbf{P}$ is the estimated contact point, $\mathbf{X}$ is the lesion centroid, and $\mathbf{d}$ is probe orientation. Probe reference system is shown in correspondence to the US sensor.

C. Preloading

The US guided biopsy procedure involves the compression of the breast not only for optimal image acquisition but also to avoid displacement of the target upon needle insertion, thus increasing the probability of successful lesion targeting. In this work, as soon as the contact point $\mathbf{P}$ is reached, the

US probe starts compressing the tissue in the direction of the target lesion until a desired force is reached. The applied force is measured by a force sensor located in the flange of the robot. In the compression phase, probe orientation is continuously adjusted to keep the target within the US image plane, as described in the following sections.

D. Deformation compensation

During preloading, breast tissue deforms under US probe compression, causing the lesion to move from its original position. To cope with this, our pipeline integrates a deformation compensation strategy that allows to continuously track lesion position $\mathbf{X}$ during compression and to adjust the probe orientation $\mathbf{d}$. To guarantee the possibility to track US occult lesions, the proposed deformation compensation strategy is based on a patient-specific biomechanical model, instead of e.g. image-based feature tracking [12], [20].

Probe-induced deformations are described using continuum mechanics laws, solved with the Finite Element Method (FEM). FEM relies on a spatial discretization of the domain, which, in our case, is achieved by creating a 3D tetrahedral mesh of the anatomy. FEM allows to solve the equations of motion on each individual element, then assembles them into a global equation system:

$$\mathbf{M}\mathbf{a} = \mathbf{f}(t, \mathbf{x}, \mathbf{v}) \tag{1}$$

where $\mathbf{x}, \mathbf{v}, \mathbf{a}$ are the position, velocity and acceleration vectors respectively, and t is time. $\mathbf{f}$ is the force vector, which includes the contribution of both internal and external forces. Internal forces depend on the constitutive model and patient-specific parameters, while external forces include any external load, e.g. gravity. $\mathbf{M}$ stands for the mass matrix.

The equation system described in (1) needs to be extended to account for the effects of the interaction between the rigid probe and the tissues. In this work, we model such interaction by imposing the impenetrability condition between the two objects as defined by Signorini's law [31]. Therefore, a term that accounts for the contribution of such constraint $\mathbf{H}^T\lambda$ is added to Eq. (1), leading to:

$$\mathbf{M}\mathbf{a} = \mathbf{f}(t, \mathbf{x}, \mathbf{v}) + \mathbf{H}^T\lambda \tag{2}$$

where $\mathbf{H}$ is the constraint matrix and λ is the vector of Lagrange multipliers, which represents the contact force. In this work, we rely on the backward Euler method for time integration and a first-order approximation of $\mathbf{f}$. A direct solver is then used to numerically solve the linearized system. In particular, the solution process is composed of three separate phases. First, eq. (2) is solved neglecting the contribution of constraints, i.e. setting $\lambda = 0$. Collision detection is then performed to detect if the first phase caused the two bodies to collide. Finally, the iterative Gauss-Seidel algorithm is used to compute the corrective motion that ensures the impenetrability condition.

By relying on constraint-based formulation, the contact condition is solved exactly. Moreover, this approach does not require prior definition of the contact surface, allowing to deal with any probe position in input. Although this approach can be computationally demanding due to the complexity of the equation system, previous work demonstrated that a good trade-off between accuracy, computation time and numerical stability can be achieved, provided that the number of elements used for spatial discretization is kept below a few thousands [22].

E. Force-position control

The robot uses a parallel force-position control. The reference force is the difference between the measured force on the end-effector and the target preloading force. The pose reference is given by the output of deformation compensation module and drives the robot towards the desired trajectory. The orientation of the end-effector is updated to maintain the estimated centroid of the suspected lesion in the plane of the US sensor while keeping the x-axis parallel to the patient's bed (Fig. 2).

The procedure ends when the desired preloading compression is reached. The final position estimated by the biomechanical model is considered as target for the biopsy.

IV. Experimental validation

The performance of the proposed pipeline with the deformation compensation is tested on the robot-assisted scanning of a realistic breast phantom.

A. Robotic setup

Our setup is shown in Fig. 1. It includes a 6-DOFs robotic arm (UR5e, Universal Robotics, Odense, Denmark) holding a MicrUS probe (Telemed, Vilnius, Lithuania) and an RGB-D camera (Intel Realsense D435, Intel Corporation, Santa Clara, CA, USA) by means of a custom-made 3D printed holder. The Tsai-Lenz hand-eye calibration algorithm [32] is used for RGB-D camera calibration. The US image is calibrated to the robot space by means of the CAD design of the holder and of the probe. This robotic setup is used to test our pipeline on a multi-modality breast phantom with some internal dense lesions of different shapes and dimensions (Model 073, CIRS, Norfolk, VA, USA). The lesions and the surrounding tissue are visible in both MRI and US.

The robot is placed on the side of the phantom, which is positioned on the stretcher in supine position. However, the presented workflow can be directly applied to the clinical setup with the patient lying prone, by positioning the robot below the stretcher so to keep the same orientation and minimize the deformation due to repositioning and gravity force. The surface models of the phantom as well as 15 internal lesions are generated from the segmentation of the pre-operative MRI of the phantom.

The breast biomechanical behavior is modelled using Neo-Hookean material law, initialized with patient-specific deformation parameters, as estimated on the same phantom used in our previous experiments [33]. The 3D model of the phantom is composed of 6,929 tetrahedral elements. Temporal discretization relies on a time step of 0.02 s. Gravity force is not included in the equation system (2) because the MRI of the phantom is acquired supine under the gravity load.

B. Experiments

The conducted experiments aim at testing the capability of the presented pipeline to position the US probe such that the suspicious lesion remains on the image plane, once the desired compression is reached. In our experiments, we run the pipeline for each lesion until the target preloading compression is applied. We repeat the experiments considering three representative magnitudes F of the preloading force (1 N, 2 N and 3 N), based on the study from [26]. For each lesion, at each preloading force level, the accuracy in probe positioning is evaluated by comparing the model-predicted lesion positions $\mathbf{X_{model}}$ with the ground truth lesion coordinates $\mathbf{X_{gt}}$.

Ground truth lesion coordinates are extracted from US images. This was possible since all the internal lesions are visible on US for the considered phantom. Lesion centroid is identified on the US image after the lesion outline is manually segmented. Thanks to the calibration, the centroid of the lesion identified in the reference of the US image can be related to its 3D coordinates $\mathbf{X_{gt}}$ in the robot space. In case the lesion cannot be visualized on the US image, once the compression is applied, due to inaccurate probe positioning, the US probe is rotated of $\pm 15\,\mathrm{deg}$ around its x-axis while keeping the contact point fixed. This condition does not introduce additional compression to the tissues, thus preventing the lesion from moving. With this motion, the US image plane sweeps a fan-shaped volume and we record images at regular steps of $0.5\,\mathrm{deg}$. We then select the US image with the largest tumor area by visual inspection of all the saved images and we extract its centroid as described before.

Localization error at preloading force F relative to tumor n is computed as Mean Squared Error (MSE):

$$MSE(F,n) = \sqrt{||\mathbf{X_{model}}(F,n) - \mathbf{X_{gt}}(f,n)||} \quad (3)$$

We compare the performance of the proposed method with deformation compensation ("DC") to adjust probe trajectory during compression, with the same pipeline but without deformation compensation ("No DC"). When no deformation compensation is applied, the orientation of the US probe is maintained constant during the entire compression, and equal to the initial orientation $\mathbf{d}$. In this case, the lesion is assumed to move with the same extent and in the same direction as the US probe.

We assess how the MSE varies depending on the probe displacement and lesion radius. Probe displacement p is defined as the distance travelled by the probe from the initial contact to the end of compression. Lesion radius is computed as the average distance of all the points on the lesion surface model and the lesion centroid, as extracted from pre-operative image.

As a final evaluation, we assess the contribution brought by the presence of the robotic manipulator with respect to manual US-guided examination. To do so, we compared our experimental results with those described in [22], where authors report a median MSE of 4.2 mm when using the same formulation described in Section III-D to model probe-induced deformations and comparable 3D mesh resolution (i.e., 7,369 elements), on freehand US scanning of the same breast phantom considered in our work. For consistent comparison, we compute the median MSE obtained when considering the same 10 lesions as in [22].

C. Results

Obtained results in terms of localization errors with and without deformation compensation are summarized in Table I. The overall accuracy of the system is influenced by each of the components of the system as follows:

- the pose accuracy of the robotic arm: $\pm$ 0.03 mm as declared by the manufacturer;
- the image acquisition error of the MicrUS probe: $\pm$ 0.078 mm;
- the calibration error between the US probe and the robotic base which depends on the resolution of the 3D printer: 0.5 mm;
- the calibration error between the RGB-D camera and the robotic arm: $\pm$ 1 mm, as given by the calibration software.

While the ground truth is influenced by the first three errors (pose, US acquisition and US calibration), therefore is submillimeter, the overall error of the system will be influenced by the registration between the reconstructed surface and the external surface of the breast, as given by the ICP algorithm after convergence. We estimated this error at around 2-3 mm averaging on all the points on the surface. However, these errors will affect both experiments we are comparing (with and without deformation compensation).

Reported values represent the median MSE achieved for all the 15 lesions, at the three considered preloading levels. Table I also reports the distance p travelled by the US probe in the different conditions and L, the lesion displacement at each force level. Probe displacement increases with the applied force as well as lesion displacement, and the obtained displacements are aligned with those of other similar works [20], [23].

A preloading force of 2 N is selected as reference for the following evaluations, since it guarantees a good trade-off between accuracy in lesion tracking and needle displacement error. Our results show that this preloading level allows to keep the median MSE (3.3 mm) below the median lesion radius (3.6 mm), thus ensuring good tracking accuracy. Previous work has demonstrated that needle targeting error is below 0.4 mm at 2 N, which does not additionally improve with larger preloading forces [26]. Moreover, the deformation compensation scheme sometimes encountered numerical instabilities when using a larger force (i.e., 3 N), due to the larger input displacement applied.

Fig. 3 reports the localization error obtained for each lesion with and without deformation compensation, depending on the lesion radius, at a preloading force of F =2 N. The obtained MSE is smaller than the radius of the corresponding lesion if it falls within the vertical gray bar, which represents lesion radius.

TABLE I: Localization error (MSE) and probe displacement (p) with deformation compensation ("DC") and without deformation compensation ("No DC") at different preloading forces. The last row –L– reports the measurements on lesion displacement at each force level. Values are in mm and expressed as median (interquartile range).

		1 N	**2 N**	**3 N**
MSE	DC	**2.8** (2.0-3.6)	**3.3** (2.7-4.2)	**3.9** (3.06-4.3)
	No DC	4.8 (3.7-5.6)	6.3 (5.3-7.0)	7.5 (6.8-8.4)
p	DC	8.3 (7.4-10.2)	14.9 (12.7-19.4)	23.9 (18.9-26.1)
	No DC	9.0 (8.0-11.5)	15.0 (13.2-18.8)	22.9 (17.9-26.4)
L	DC	5.3 (4.7-7.1)	10.9 (8.8-14.0)	18.8 (14.0-20.5)
	No DC	6.2 (5.0-7.8)	11.0 (9.2-13.8)	17.3 (12.3-20.64)

In Fig. 4 we report the localization error, with and without compensation, against the movement of the probe to analyze if there is a correlation between the distance traveled by the probe from the first contact **P** to the final position.

Finally, the median MSE obtained at a preloading of 2 N when considering the same 10 internal lesions as [22] is 3.34 mm.

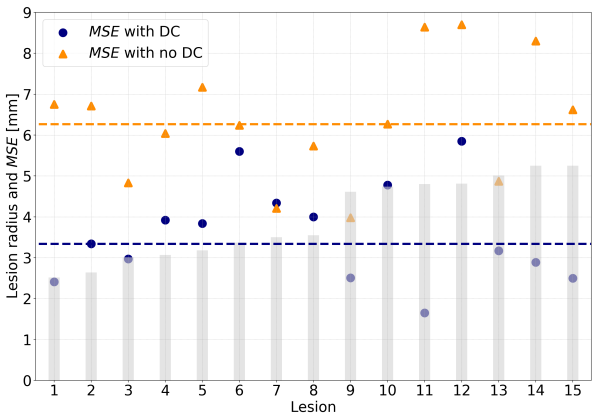

Fig. 3: Localization error for each lesion with and without deformation compensation, at a preloading force of 2N. Horizontal dashed lines represent median error values over all the lesions. Lesions are reported in ascending order depending on lesion radius, which is represented by the gray vertical bars.

V. Discussion

This work presents a complete robotic setup for US-guided breast biopsy that is able to autonomously perform all the steps from initial registration with pre-operative MRI data to final US probe positioning, just before needle insertion. The prototype we described here operates in assistive mode at autonomy level 2 (Task Autonomy), according to the classification given in [34], and at LoA 2 (Task-level autonomy) according to [16]. The main innovative contribution of the system is the integration of two fundamental components: preloading technique for minimization of needle insertion error, and a deformation compensation scheme for lesion tracking during tissues compression.

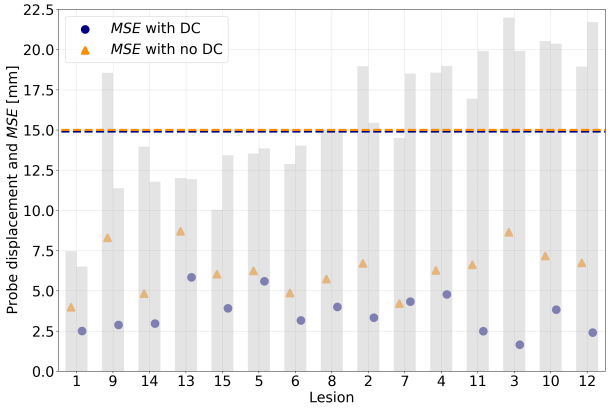

Fig. 4: Localization error for each lesion with and without deformation compensation, at a preloading force of 2N. Horizontal dashed lines represent median probe displacement over all the lesions. Lesions are reported in ascending order depending on probe displacement, which is represented by the gray vertical bars. This order is chosen to facilitate visualization of the relationship between probe penetration and simulation error. The number of each lesion is kept consistent with that used in Fig. 3.

The presence of the deformation compensation scheme allows to improve the tracking of internal targets during compression. Obtained results in terms of lesion localization accuracy, when using our pipeline, outperform those obtained when the deformation compensation scheme is not used for all the considered preloading forces, with an improvement of 48% at both 2 and 3 N (Table I). Fig. 3 and 4 show that the deformation compensation strategy allows to improve the localization accuracy for all the considered lesions except one (where the error is aligned with the one obtained without deformation compensation). This exception is due to the position of the lesion in question, which is located in the lowest part of the phantom, close to the boundary conditions (our method assumes that the points on the boundary do not move). Accurate lesion tracking is essential to position the US probe such that the lesion remains on the US image plane, ensuring an optimal view on both the target and the needle during biopsy.

Combining the obtained results with the findings from previous work [26], we can conclude that the best trade-off between the localization error and the needle targeting error can be achieved using a preloading force of 2 N. Such force allows also to minimize the applied tissue stress. When relying on a preloading of 2 N, we are able to keep the lesion localization error below lesion radius in 7 out of 15 lesions, whereas this happens for 2 lesions only when the deformation compensation scheme is not used (Fig. 3). It is worth highlighting that the presence of the deformation model is fundamental to limit the error in case of the smallest lesions, which are the most challenging to track and generally the most difficult to be visualized in US images. Internal lesions are visible in US images in the considered phantom

since they were necessary to provide ground truth lesion positions during tissue compression. However, by relying on a deformation model, our pipeline does not require lesions to be visible on the US images but it is sufficient to know their initial position from the pre-operative MRI. Moreover, Fig. 4 shows that our method allows to keep the error limited even for large input deformations, i.e. around 20 mm.

The improved accuracy could be reached thanks to the use of patient-specific parameterization of the deformation model, which was available for the considered phantom. In the real clinical practice, deformation parameters can be either initialized with values obtained from the literature or they can be estimated using dedicated imaging (e.g. elastography [35]) or analytically [36].

The localization error obtained with the proposed robotic system improves the one obtained by [22] on a similar experimental setup, but on freehand scanning. Improvement in the results can be explained by the presence of the robotic manipulator, which enhances the precision in tracking and positioning of the US probe, and measuring the applied force.

The main limitation of the conducted experimental evaluation is that needle insertion is not performed in the conducted experiments to avoid introducing irreversible damages to the phantom. However, the contribution of the presented pipeline with deformation compensation could be assessed even without including the biopsy phase. Although we could not directly assess the needle targeting error, we assume that such error is bounded thanks to the preloading technique, as reported in [26].

VI. Conclusion

In this work we demonstrated how a robotic system with deformation compensation may overcome the limitations of the standard breast biopsy procedure in targeting lesions that potentially are not seen in the US image. This system is prepared for needle insertion with minimal displacement thanks to the preloading technique. The integration of a deformation model proves fundamental to improve US probe positioning during compression, to maintain the target within the US image plane.

This first prototype focused on the validation of the deformation compensation while reaching a target. The other components of the system (e.g. external surface acquisition and registration) will be refined in future works in order to allow to the robot to reach an accuracy below the lesion radius for all targets.

In future works, we will improve the experimental validation by including the needle insertion phase to assess needle targeting error. Moreover, we will investigate the use of the deformation model to compensate for needle-induced deformations as well. Toward the clinical implementation, the next step on the development of our system will be to measure the force applied by a physician during an US guided breast biopsy, so to assess whether the literature assumption of a 2N pressure is compliant with the clinical practice. The understanding of the forces involved in the breast biopsy and the possibility to measure them in a robotic guided procedure, may also play a role in the overall safety of the intervention.

References

[1] H. Sung, *et al.*, "Global cancer statistics 2020: Globocan estimates of incidence and mortality worldwide for 36 cancers in 185 countries," *A Cancer Journal for Clinicians*, vol. 71, no. 3, pp. 209–249, 2021.

[2] V. Papalouka, F. Kilburn-Toppin, M. Gaskarth, and F. Gilbert, "Mri-guided breast biopsy: a review of technique, indications, and radiological–pathological correlations," *Clinical radiology*, vol. 73, no. 10, pp. 908–e17, 2018.

[3] A. C. of Radiology *et al.*, "Acr practice parameter for the performance of ultrasound-guided percutaneous breast interventional procedures," 2017.

[4] Y. Gao, B. Reig, L. Heacock, D. L. Bennett, S. L. Heller, and L. Moy, "Magnetic resonance imaging in screening of breast cancer," *Radiologic Clinics*, vol. 59, no. 1, pp. 85–98, 2021.

[5] D. Rueckert, L. Sonoda, C. Hayes, D. Hill, M. Leach, and D. Hawkes, "Nonrigid registration using free-form deformations: application to breast mr images," *IEEE Transactions on Medical Imaging*, vol. 18, no. 8, pp. 712–721, 1999.

[6] M. Danch-Wierzchowska, D. Borys, and A. Swierniak, "Breast deformation modeling based on mri images, preliminary results," in *Conference of Information Technologies in Biomedicine*. Springer, 2016, pp. 227–234.

[7] F. J. Siepel, B. Maris, M. K. Welleweerd, V. Groenhuis, P. Fiorini, and S. Stramigioli, "Needle and biopsy robots: A review," *Current Robotics Reports*, vol. 2, no. 1, pp. 73–84, 2021.

[8] F. von Haxthausen, S. Böttger, D. Wulff, J. Hagenah, V. García-Vázquez, and S. Ipsen, "Medical robotics for ultrasound imaging: current systems and future trends," *Current Robotics Reports*, vol. 2, no. 1, pp. 55–71, 2021.

[9] B. Maris, *et al.*, "Preclinical validation of a semi-autonomous robot for transperineal prostate biopsy," *IEEE Transactions on Medical Robotics and Bionics*, vol. 4, no. 2, pp. 311–322, 2022.

[10] M. Z. Mahmoud, M. Aslam, M. Alsaadi, M. A. Fagiri, and B. Alonazi, "Evolution of robot-assisted ultrasound-guided breast biopsy systems," *Journal of radiation research and applied sciences*, vol. 11, no. 1, pp. 89–97, 2018.

[11] G. Fichtinger, J. Troccaz, and T. Haidegger, "Image-guided interventional robotics: Lost in translation?" *Proceedings of the IEEE*, 2022.

[12] M. K. Welleweerd, A. G. de Groot, S. de Looijer, F. J. Siepel, and S. Stramigioli, "Automated robotic breast ultrasound acquisition using ultrasound feedback," in *2020 IEEE Int. Conf. on Robotics and Automation (ICRA)*. IEEE, 2020, pp. 9946–9952.

[13] N. Wöhrle, K. Hellerhoff, M. Notohamiprodjo, M. Reiser, and D.-A. Clevert, "Automated-breast-volume-scanner (abvs)," *Der Radiologe*, vol. 50, no. 11, pp. 973–981, 2010.

[14] A. V. Nikolaev, *et al.*, "Quantitative evaluation of an automated cone-based breast ultrasound scanner for mri–3d us image fusion," *IEEE transactions on medical imaging*, vol. 40, no. 4, pp. 1229–1239, 2021.

[15] B. Maris, *et al.*, "Toward autonomous robotic prostate biopsy: a pilot study," *International Journal of Computer Assisted Radiology and Surgery*, vol. 16, no. 8, pp. 1393–1401, 2021.

[16] T. Haidegger, "Autonomy for surgical robots: Concepts and paradigms," *IEEE Transactions on Medical Robotics and Bionics*, vol. 1, no. 2, pp. 65–76, 2019.

[17] P. Fiorini, K. Y. Goldberg, Y. Liu, and R. H. Taylor, "Concepts and trends in autonomy for robot-assisted surgery," *Proceedings of the IEEE*, vol. 110, no. 7, pp. 993–1011, 2022.

[18] Z. Jiang, Y. Zhou, Y. Bi, M. Zhou, T. Wendler, and N. Navab, "Deformation-aware robotic 3d ultrasound," *IEEE Robotics and Automation Letters*, vol. 6, no. 4, pp. 7675–7682, 2021.

[19] S. Virga, *et al.*, "Automatic force-compliant robotic ultrasound screening of abdominal aortic aneurysms," in *2016 IEEE/RSJ Int. Conf. on intelligent robots and systems (IROS)*. IEEE, 2016, pp. 508–513.

[20] M. K. Welleweerd, D. Pantelis, A. G. de Groot, F. J. Siepel, and S. Stramigioli, "Robot-assisted ultrasound-guided biopsy on mr-detected breast lesions," in *2020 IEEE/RSJ Int. Conf. on Intelligent Robots and Systems (IROS)*. IEEE, 2020, pp. 2965–2971.

[21] E. Tagliabue, D. Dall'Alba, E. Magnabosco, C. Tenga, I. Peterlik, and P. Fiorini, "Position-based modeling of lesion displacement in ultrasound-guided breast biopsy," *Int. Jour. of computer assisted radiology and surgery*, vol. 14, no. 8, pp. 1329–1339, 2019.

[22] E. Tagliabue, D. Dall'Alba, E. Magnabosco, I. Peterlik, and P. Fiorini, "Biomechanical modelling of probe to tissue interaction during ultrasound scanning," *Int. Jour. of Computer Assisted Radiology and Surgery*, vol. 15, no. 8, pp. 1379–1387, 2020.

[23] V. Groenhuis, *et al.*, "Deformation compensation in robotically-assisted breast biopsy," in *11th Int. Conf. on Information Processing in Computer-Assisted Interventions, IPCAI 2020*, 2020.

[24] M. Lagomarsino, V. Groenhuis, M. Casadio, M. K. Welleweerd, F. J. Siepel, and S. Stramigioli, "Image-guided breast biopsy of mri-visible lesions with a hand-mounted motorised needle steering tool," in *2021 International Symposium on Medical Robotics (ISMR)*. IEEE, 2021, pp. 1–7.

[25] V. G. Mallapragada, N. Sarkar, and T. K. Podder, "Robot-assisted real-time tumor manipulation for breast biopsy," *IEEE Transactions on Robotics*, vol. 25, no. 2, pp. 316–324, 2009.

[26] Y. Kobayashi, *et al.*, "Enhanced targeting in breast tissue using a robotic tissue preloading-based needle insertion system," *IEEE Transactions on Robotics*, vol. 28, no. 3, pp. 710–722, 2012.

[27] Y. Madjidi, *et al.*, "Experimental platform for intra-uterine needle placement procedures," in *Medical Imaging 2013: Image-Guided Procedures, Robotic Interventions, and Modeling*, vol. 8671. SPIE, 2013, pp. 414–421.

[28] P. A. Yushkevich, *et al.*, "User-guided 3D active contour segmentation of anatomical structures: Significantly improved efficiency and reliability," *Neuroimage*, vol. 31, no. 3, pp. 1116–1128, 2006.

[29] Z. H. Al-Tairi, R. W. Rahmat, M. I. Saripan, and P. S. Sulaiman, "Skin segmentation using yuv and rgb color spaces," *Journal of information processing systems*, vol. 10, no. 2, pp. 283–299.

[30] K. S. Arun, T. S. Huang, and S. D. Blostein, "Least-squares fitting of two 3-d point sets," *IEEE Transactions on Pattern Analysis and Machine Intelligence*, vol. PAMI-9, no. 5, pp. 698–700, 1987.

[31] C. Duriez, C. Andriot, and A. Kheddar, "Signorini's contact model for deformable objects in haptic simulations," in *Intelligent Robots and Systems, 2004.(IROS 2004). Proceedings. 2004 IEEE/RSJ Int. Conf. on*, vol. 4. IEEE, 2004, pp. 3232–3237.

[32] R. K. L. Roger Y. Tsai, "Real time versatile robotics hand/eye calibration using 3d machine vision," *IEEE Int. Conf. on Robotics and Automation*, vol. 1, no. 10.1109/ROBOT.1988.12110, pp. 554–561, 1988.

[33] F. Visentin, *et al.*, "Iterative simulations to estimate the elastic properties from a series of mri images followed by mri-us validation," *Medical & biological engineering & computing*, vol. 57, no. 4, pp. 913–924, 2019.

[34] G.-Z. Yang, *et al.*, "Medical robotics—regulatory, ethical, and legal considerations for increasing levels of autonomy," p. eaam8638, 2017.

[35] J. Ormachea and K. Parker, "Elastography imaging: the 30 year perspective," *Physics in Medicine & Biology*, vol. 65, no. 24, p. 24TR06, 2020.

[36] V. Groenhuis, *et al.*, "Analytical derivation of elasticity in breast phantoms for deformation tracking," *International journal of computer assisted radiology and surgery*, vol. 13, no. 10, pp. 1641–1650, 2018.